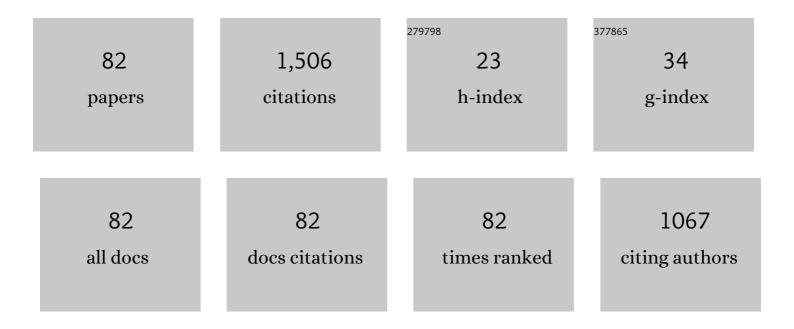
List of Publications by Year in descending order

Source: https://exaly.com/author-pdf/4698183/publications.pdf Version: 2024-02-01



LIDI HOLISKA

#	Article	IF	CITATIONS
1	Dependence of the ZrO2 growth on the crystal orientation: growth simulations and magnetron sputtering. Applied Surface Science, 2022, 572, 151422.	6.1	9
2	Vacancies and substitutional defects in multicomponent diboride Ti _{0.25} Zr _{0.25} Hf _{0.25} Ta _{0.25} B ₂ : first-principle study. Journal of Physics Condensed Matter, 2022, 34, 095901.	1.8	3
3	Transfer of the sputter technique for deposition of strongly thermochromic VO2-based coatings on ultrathin flexible glass to large-scale roll-to-roll device. Surface and Coatings Technology, 2022, 442, 128273.	4.8	10
4	Design and reactive magnetron sputtering of thermochromic coatings. Journal of Applied Physics, 2022, 131, .	2.5	19
5	Multifunctional MoOx and MoOxNy films with 2.5 < x < 3.0 and y < 0.2 prepared using controlled reactive deep oscillation magnetron sputtering. Thin Solid Films, 2021, 717, 138442.	1.8	Ο
6	Enhancement of high-temperature oxidation resistance and thermal stability of hard and optically transparent Hf–B–Si–C–N films by Y or Ho addition. Journal of Non-Crystalline Solids, 2021, 553, 120470.	3.1	3
7	Dependence of characteristics of Hf(M)SiBCN (MÂ=ÂY, Ho, Ta, Mo) thin films on the M choice: Ab-initio and experimental study. Acta Materialia, 2021, 206, 116628.	7.9	7
8	Toward colorless smart windows. Solar Energy Materials and Solar Cells, 2021, 230, 111210.	6.2	4
9	Hard and electrically conductive multicomponent diboride-based films with high thermal stability. Ceramics International, 2021, , .	4.8	4
10	Microstructure of high-performance thermochromic ZrO2/V0.984W0.016O2/ZrO2 coating with a low transition temperature (22°C) prepared on flexible glass. Surface and Coatings Technology, 2021, 424, 127654.	4.8	7
11	Maximum Achievable N Content in Atom-by-Atom Growth of Amorphous Si-B-C-N Materials. Materials, 2021, 14, 5744.	2.9	2
12	High-performance thermochromic VO2-based coatings with a low transition temperature deposited on glass by a scalable technique. Scientific Reports, 2020, 10, 11107.	3.3	29
13	Maximum Achievable N Content in Atom-by-Atom Growth of Amorphous Si–C–N. ACS Applied Materials & Interfaces, 2020, 12, 41666-41673.	8.0	2
14	Pulsed Magnetron Sputtering of Strongly Thermochromic VO2-Based Coatings with a Transition Temperature of 22 A°C onto Ultrathin Flexible Glass. Coatings, 2020, 10, 1258.	2.6	11
15	Bixbyite-Ta2N2O film prepared by HiPIMS and postdeposition annealing: Structure and properties. Journal of Vacuum Science and Technology A: Vacuum, Surfaces and Films, 2020, 38, .	2.1	1
16	Molecular dynamics and experimental study of the growth, structure and properties of Zr–Cu films. Journal of Alloys and Compounds, 2020, 828, 154433.	5.5	12
17	Self-organization of vapor-deposited polyolefins at the solid/vacuum interface. Progress in Organic Coatings, 2020, 143, 105630.	3.9	5
18	Tunable composition and properties of Al-O-N films prepared by reactive deep oscillation magnetron sputtering. Surface and Coatings Technology, 2020, 392, 125716.	4.8	5

#	Article	IF	CITATIONS
19	Extraordinary high-temperature behavior of electrically conductive Hf7B23Si22C6N40 ceramic film. Surface and Coatings Technology, 2020, 391, 125686.	4.8	5
20	Distribution of O atoms on partially oxidized metal targets, and the consequences for reactive sputtering of individual metal oxides. Surface and Coatings Technology, 2020, 392, 125685.	4.8	5
21	Maximum N content in a-CNx by ab-initio simulations. Acta Materialia, 2019, 174, 189-194.	7.9	5
22	Effect of energetic particles on pulsed magnetron sputtering of hard nanocrystalline MBCN (M =†Ti, Zr,) Tj E	TQq0 0 0 1.8	rgBT /Overloo
23	High-rate reactive high-power impulse magnetron sputtering of transparent conductive Al-doped ZnO thin films prepared at ambient temperature. Thin Solid Films, 2019, 679, 35-41.	1.8	12
24	Effect of annealing on structure and properties of Ta–O–N films prepared by high power impulse magnetron sputtering. Ceramics International, 2019, 45, 9454-9461.	4.8	10
25	Significant improvement of the performance of ZrO2/V1-W O2/ZrO2 thermochromic coatings by utilizing a second-order interference. Solar Energy Materials and Solar Cells, 2019, 191, 365-371.	6.2	46
26	Tribological properties and oxidation resistance of tungsten and tungsten nitride films at temperatures up to 500â€Â°C. Tribology International, 2019, 132, 211-220.	5.9	20
27	Ion-flux characteristics during low-temperature (300 °C) deposition of thermochromic VO ₂ films using controlled reactive HiPIMS. Journal Physics D: Applied Physics, 2019, 52, 025205.	2.8	10
28	Thermal stability of structure, microstructure and enhanced properties of Zr–Ta–O films with a low and high Ta content. Surface and Coatings Technology, 2018, 335, 95-103.	4.8	5
29	Magnetron sputtered Hf–B–Si–C–N films with controlled electrical conductivity and optical transparency, and with ultrahigh oxidation resistance. Thin Solid Films, 2018, 653, 333-340.	1.8	14
30	Enhancement of the deposition rate in reactive mid-frequency ac magnetron sputtering of hard and optically transparent ZrO 2 films. Surface and Coatings Technology, 2018, 336, 54-60.	4.8	12
31	In-Ga-Zn-O thin films with tunable optical and electrical properties prepared by high-power impulse magnetron sputtering. Thin Solid Films, 2018, 658, 27-32.	1.8	8
32	Properties of thermochromic VO2 films prepared by HiPIMS onto unbiased amorphous glass substrates at a low temperature of 300â€ ⁻ °C. Thin Solid Films, 2018, 660, 463-470.	1.8	26
33	Improved performance of thermochromic VO2/SiO2 coatings prepared by low-temperature pulsed reactive magnetron sputtering: Prediction and experimental verification. Journal of Alloys and Compounds, 2018, 767, 46-51.	5.5	24
34	Structure and properties of Hf-O-N films prepared by high-rate reactive HiPIMS with smoothly controlled composition. Ceramics International, 2017, 43, 5661-5667.	4.8	22
35	Strong effect of the interaction potential cut-off on the crystallinity of films grown by simulations. Molecular Simulation, 2017, 43, 1436-1441.	2.0	0
36	Relationships between the distribution of O atoms on partially oxidized metal (Al, Ag, Cu, Ti, Zr, Hf) surfaces and the adsorption energy: A density-functional theory study. Journal of Applied Physics, 2017, 121, 225303.	2.5	6

#	Article	IF	CITATIONS
37	Force field for realistic molecular dynamics simulations of TiO 2 growth. Computational Materials Science, 2017, 134, 1-7.	3.0	3
38	Reactive high-power impulse magnetron sputtering of ZrO2 films with gradient ZrOx interlayers on pretreated steel substrates. Journal of Vacuum Science and Technology A: Vacuum, Surfaces and Films, 2017, 35, 031503.	2.1	7
39	Controlled reactive HiPIMS—effective technique for low-temperature (300 °C) synthesis of VO ₂ films with semiconductor-to-metal transition. Journal Physics D: Applied Physics, 2017, 50, 38LT01.	2.8	38
40	Characterization of thermochromic VO2 (prepared at 250 ŰC) in a wide temperature range by spectroscopic ellipsometry. Applied Surface Science, 2017, 421, 529-534.	6.1	34
41	Molecular dynamics study of the growth of crystalline ZrO2. Surface and Coatings Technology, 2016, 304, 23-30.	4.8	15
42	Microstructure of hard and optically transparent HfO2 films prepared by high-power impulse magnetron sputtering with a pulsed oxygen flow control. Thin Solid Films, 2016, 619, 239-249.	1.8	25
43	Dependence of characteristics of MSiBCN (M = Ti, Zr, Hf) on the choice of metal element: Experimental and ab-initio study. Thin Solid Films, 2016, 616, 359-365.	1.8	14
44	Thermal, mechanical and electrical properties of hard B4C, BCN, ZrBC and ZrBCN ceramics. Ceramics International, 2016, 42, 4361-4369.	4.8	20
45	High-rate reactive high-power impulse magnetron sputtering of hard and optically transparent HfO 2 films. Surface and Coatings Technology, 2016, 290, 58-64.	4.8	49
46	Force field for realistic molecular dynamics simulations of ZrO 2 growth. Computational Materials Science, 2016, 111, 209-217.	3.0	13
47	Effect of the Si content on the microstructure of hard, multifunctional Hf–B–Si–C films prepared by pulsed magnetron sputtering. Applied Surface Science, 2015, 357, 1343-1354.	6.1	20
48	Thermal stability and transformation phenomena in magnetron sputtered Al–Cu–O films. Ceramics International, 2015, 41, 6020-6029.	4.8	3
49	Dependence of structure and properties of hard nanocrystalline conductive films MBCN (M = Ti, Zr,) Tj ETQq1 1	0.784314 1.8	∙rgBT /Overl⊂
50	Ageing resistance of SiBCN ceramics. Ceramics International, 2015, 41, 7921-7928.	4.8	5
51	Benefits of the controlled reactive high-power impulse magnetron sputtering of stoichiometric ZrO2 films. Vacuum, 2015, 114, 131-141.	3.5	56
52	Hard multifunctional Hf–B–Si–C films prepared by pulsed magnetron sputtering. Surface and Coatings Technology, 2014, 257, 301-307.	4.8	20
53	A study of the microstructure evolution of hard Zr–B–C–N films by high-resolution transmission electron microscopy. Acta Materialia, 2014, 77, 212-222.	7.9	25
54	High-rate reactive high-power impulse magnetron sputtering of Ta–O–N films with tunable composition and properties. Thin Solid Films, 2014, 566, 70-77.	1.8	29

#	Article	IF	CITATIONS
55	Quantitative investigation of the role of high-energy particles in Al2O3 thin film growth: A molecular-dynamics study. Surface and Coatings Technology, 2014, 254, 131-137.	4.8	13
56	Trends in formation energies and elastic moduli of ternary and quaternary transition metal nitrides. Journal of Materials Science, 2013, 48, 7642-7651.	3.7	25
57	Effect of N and Zr content on structure, electronic structure and properties of ZrBCN materials: An ab-initio study. Thin Solid Films, 2013, 542, 225-231.	1.8	14
58	Process stabilization and a significant enhancement of the deposition rate in reactive high-power impulse magnetron sputtering of ZrO2 and Ta2O5 films. Surface and Coatings Technology, 2013, 236, 550-556.	4.8	72
59	Pathway for a low-temperature deposition of α-Al2O3: A molecular dynamics study. Surface and Coatings Technology, 2013, 235, 333-341.	4.8	30
60	Pulsed reactive magnetron sputtering of high-temperature Si–B–C–N films with high optical transparency. Surface and Coatings Technology, 2013, 226, 34-39.	4.8	22
61	Experimental and molecular dynamics study of the growth of crystalline TiO2. Journal of Applied Physics, 2012, 112, 073527.	2.5	29
62	Stress reduction in cubic boron nitride by oxygen addition: Explanation of the mechanism by ab-initio simulations. Surface and Coatings Technology, 2012, 206, 2541-2544.	4.8	2
63	Overview of optical properties of Al2O3 films prepared by various techniques. Thin Solid Films, 2012, 520, 5405-5408.	1.8	53
64	Ab initiomodeling of complex amorphous transition-metal-based ceramics. Journal of Physics Condensed Matter, 2011, 23, 025502.	1.8	8
65	Properties of nanocrystalline Al–Cu–O films reactively sputtered by DC pulse dual magnetron. Applied Surface Science, 2011, 258, 1762-1767.	6.1	36
66	Effect of nitrogen content on electronic structure and properties of SiBCN materials. Acta Materialia, 2011, 59, 2341-2349.	7.9	36
67	SiBCN materials for high-temperature applications: Atomistic origin of electrical conductivity. Journal of Applied Physics, 2010, 108, .	2.5	9
68	Atom-by-atom simulations of chemical vapor deposition of nanoporous hydrogenated silicon nitride. Journal of Applied Physics, 2010, 107, .	2.5	22
69	Relationships between composition and properties of (Cr/Ti)SiN and (Cr/Ti)CN alloys: anab initiostudy. Journal of Physics Condensed Matter, 2009, 21, 285302.	1.8	7
70	Atomistic simulations of the characteristics of TiSiN nanocomposites of various compositions. Surface and Coatings Technology, 2009, 203, 3348-3355.	4.8	35
71	Formation and behavior of unbonded hydrogen in a-C:H of various compositions and densities. Surface and Coatings Technology, 2009, 203, 3770-3776.	4.8	15
72	Mechanical and optical properties of quaternary Si–B–C–N films prepared by reactive magnetron sputtering. Thin Solid Films, 2008, 516, 7286-7293.	1.8	23

#	Article	IF	CITATIONS
73	Effect of the gas mixture composition on high-temperature behavior of magnetron sputtered Si–B–C–N coatings. Surface and Coatings Technology, 2008, 203, 466-469.	4.8	42
74	Effect of implanted argon on hardness of novel magnetron sputtered Si–B–C–N materials: experiments andab initiosimulations. Journal of Physics Condensed Matter, 2007, 19, 196228.	1.8	17
75	Bonding statistics and electronic structure of novel Si–B–C–N materials: <i>Ab initio</i> calculations and experimental verification. Journal of Vacuum Science and Technology A: Vacuum, Surfaces and Films, 2007, 25, 1411-1416.	2.1	21
76	Influence of substrate bias voltage on structure and properties of hard Si–B–C–N films prepared by reactive magnetron sputtering. Diamond and Related Materials, 2007, 16, 29-36.	3.9	55
77	lon-bombardment characteristics during deposition of TiN films using a grid-assisted magnetron system with enhanced plasma potential. Vacuum, 2007, 81, 1109-1113.	3.5	6
78	Effect of B and the Si/C ratio on high-temperature stability of Si–B–C–N materials. Europhysics Letters, 2006, 76, 512-518.	2.0	34
79	The effect of argon on the structure of amorphous SiBCN materials: an experimental andab initiostudy. Journal of Physics Condensed Matter, 2006, 18, 2337-2348.	1.8	19
80	A study on the energy distribution for grid-assisting magnetron sputtering. Surface and Coatings Technology, 2005, 200, 421-424.	4.8	4
81	Ab initiosimulations of nitrogen evolution in quenchedCNxand SiBCN amorphous materials. Physical Review B, 2005, 72, .	3.2	25
82	Reactive magnetron sputtering of hard Si–B–C–N films with a high-temperature oxidation resistance. Journal of Vacuum Science and Technology A: Vacuum, Surfaces and Films, 2005, 23, 1513-1522.	2.1	76